

SYLWESTER RAJWA<sup>1\*</sup>, SVEN BOCK<sup>2</sup>**OPTIMISATION OF SELECTED PARAMETERS OF THE SHIELD SUPPORT BASE DEDICATED FOR THE CONDITION OF A WEAK FLOOR**

In longwall coal exploitation, problems with the proper functioning of the powered shield support often occur. In many cases, it results from the insufficient load-bearing capacity of the ground (floor) and the inability to achieve the set or yield pressure of the shield support. The improper functioning of the shield support may also result from its construction and the lack of optimisation to work effectively on a weak mine floor. This paper presents an attempt to optimise the operating conditions of the base of two-legged shield support based on the field observations and results of the PFC3D numerical calculation. In the framework of the numerical calculations, the impact of the width of the base and the location of the hydraulic legs on the working conditions of shield support on a weak floor were analysed.

**Keywords:** numerical modelling; PFC3D; weak floor; shield support; longwall mining

## 1. Introduction

Coal exploitation in Polish mines is almost exclusively realised using longwalls. For several years, GIG (Central Mining Institute) has been conducting underground observation and measurements of the roof and floor stability in the area of a coal face [1-3]. This research has confirmed that the possibility of decreasing the stability of workings depends on the proper functioning of shield support with the rock mass [4-8]. Significant disturbances in the longwall advancement occur particularly often in cases of the low load-bearing capacity of the floor (weak floor). The load-bearing capacity is often defined as the maximum load acting on the floor until the limit state is achieved and a significant drop in the bearing capacity occurs due to brittle destruction or

<sup>1</sup> CENTRAL MINING INSTITUTE (GIG), 1 GWARKÓW SQ., 40-166 KATOWICE, POLAND

<sup>2</sup> DMT GMBH, GERMANY

\* Corresponding author: [srajwa@gig.eu](mailto:srajwa@gig.eu)



© 2022. The Author(s). This is an open-access article distributed under the terms of the Creative Commons Attribution-NonCommercial License (CC BY-NC 4.0, <https://creativecommons.org/licenses/by-nc/4.0/deed.en>) which permits the use, redistribution of the material in any medium or format, transforming and building upon the material, provided that the article is properly cited, the use is noncommercial, and no modifications or adaptations are made.

plastic yielding [9-12]. This parameter is of great importance not only in the longwall exploitation [13-16], but also in the room and pillar method [17,18].

The load-bearing capacity may be obtained from results of underground or laboratory measurements using special devices [11,19-23], or utilising empirical, analytical or numerical analysis [9,14,17,24-27]. Currently, in Polish coal mines, such underground measurements are no longer conducted and load-bearing capacity is often assessed using empirical and analytical dependencies developed for soils. The reason for this approach is the similarity of the soil and the weak floor, floor loaded to above its stress limit or clay type floor under the influence of water. A decrease in the strength properties of the floor often occurs during the downtime of a longwall, especially for a clay type floor, when the natural or technological water may penetrate the floor's layers. This phenomenon is facilitated due to cracks in the rock mass around the coal face resulting from the longwall advance [28]. The saturation of the floor's layers leads to a decrease in the parameters which are important for load-bearing capacity. Underground and laboratory tests show that the decrease of the strength of clay type rocks is significant, and in some cases, the final compressive strength may only be 10%-20% of the initial value [14,29].

Sustained or excessive water inflow into clay type floor layers leads initially to their softening and finally to the sinking of the shield support and crowding out of the floor from below the base of working shield support. As a result, severe disturbance to longwall advance may occur (Fig. 1). To avoid these phenomena, it is advisable to periodically reset the shield support during downtime. Such an approach allows limiting the support yielding at the contact point of a canopy and roof resulting from floor failure.

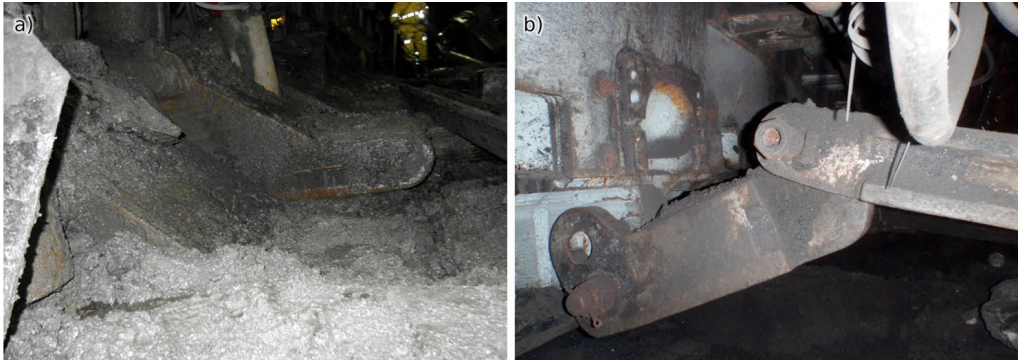


Fig. 1. Disturbances in longwall advance in conditions of a saturated weak floor: a) sinking of the base of shield support, b) lifting of the relay bar as a result of base sinking [4]

Another negative phenomenon is the loss of the proper geometry of the shield support due to the crowding out of the floor layers from below the base. Asymmetry in the load of the shield support (the canopy only partially supports the roof) leads to an increase in the destruction of the surrounding rock mass and further disturbances in maintaining the stability of the shield support [30].

Due to the above problems of maintaining shield support stability, numerical calculations using the commercial software Particle Flow Code in 3D v. 4.0 (PFC3D) [31] were performed to analyse the possibility of geometry loss and construction optimisation of the base of the shield

support in conditions of a weak floor. The numerical model allows a simplified way of modelling the base of the shield support. Nevertheless, even such a simple calculation enables an understanding of phenomena occurring between the base and the weak floor.

## 2. Material and Methods

By default in PFC3D, all contacts between the ball(s) and walls are assigned either the linear or Hertz model. The following component behaviours describe the contacts (PFC3D User Manual – Theory and Background – Contact models) [31]:

- Stiffness – relates to contact forces and relative displacements in the normal and shear directions.
- Slip behaviour – provided by enforcing a relationship between shear and normal force so that the two contacting entities may slip relative to one another.
- Bonding behaviour (contact and parallel bonds) – a way of joining two particles that could be envisioned as a type of glue. In the contact bond, the glue is of a vanishingly small size that acts only at the contact point, while the parallel-bond glue is of a finite size that acts over the area lying between the particles. Both types of bonds may be active at the same time until the specific bond is broken.
- For the numerical simulation, it was assumed that due to the interaction between the weak rock mass and the base of the shield support the floor is already disintegrated and cracked. Therefore a contact model with a relatively simple relationship between the micro and macro properties of grains was chosen. The contact bond, defined by normal  $F_c^n$  and shear  $F_c^s$  bond strengths, acts at the contact point. The bond can break in two cases: the magnitude of the tensile normal contact force equals or exceeds the normal contact bond strength, or the magnitude of the shear contact force equals or exceeds the shear contact bond strength. In the first case, the normal and shear contact forces are set to zero. In the second case the contact forces are altered only if shear force exceeds the friction limit and the normal force is tensile ( $F^n < 0$ ). The micro properties of the weak floor are shown in Table 1.

TABLE 1

Micro properties of the weak floor

Parameter	Value
Ball normal stiffness, Pa	1e7
Ball shear stiffness, Pa	1e7
Friction coefficient	0.7
Contact bond normal stiffness, Pa	1e6
Contact bond shear stiffness, Pa	1e6
Contact bond tensile strength, N	5e6
Contact bond shear strength, N	5e6
Density of material, kg/m <sup>3</sup>	2000
Critical damping ratio $\beta$	0.7
Target porosity	0.1
Min. radius of particles forming the floor, mm	90
Max. radius of particles forming the floor, mm	160

The micro properties of the weak floor, presented in table 1, were chosen based on previous experience using PFC3D. To ensure the precise calculations of the resulting macro properties of the floor, a function for assessing the mechanical properties of a specimen, provided by Itasca, was used (Granular.p2prtj). As a result of the numerical simulation of the strength test, plots of strain-stress were obtained (Fig. 2), and the UCS and residual UCS of the floor was estimated as equal to 3.0 MPa and 2.3 MPa, respectively.

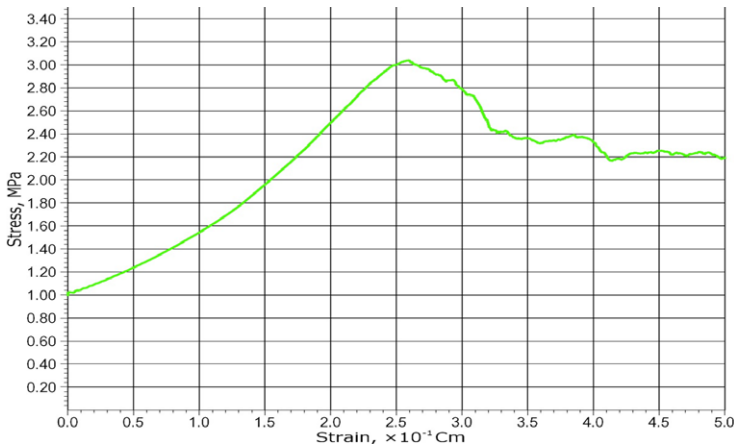


Fig. 2. Stress vs. strain curve for the analysed weak floor

For the determination of elastic properties, a procedure of loading/unloading tests under elastic conditions was used (LoadUnload.p2dat). Plots of axial deviatoric stress and volumetric strain versus axial strain are shown for the dense specimen in Figs 3 and 4.

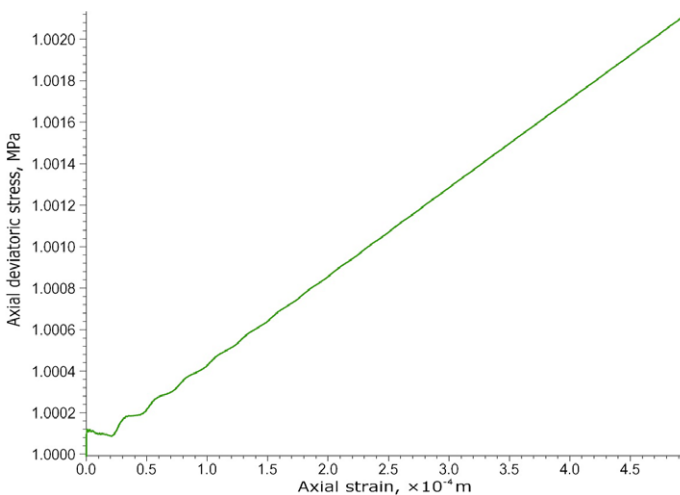


Fig. 3. Axial deviatoric stress vs. axial strain for elastic load/unload test

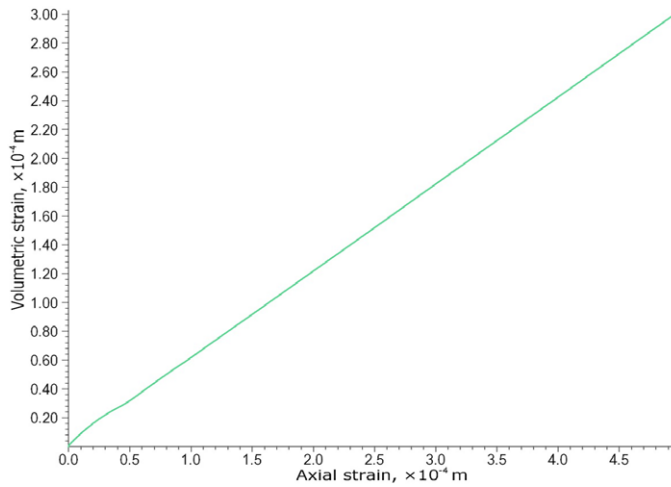


Fig. 4. Volumetric strain vs. axial strain for elastic load/unload test

From these plots Young's modulus, Poisson's ratio and shear modulus can be estimated using the following expressions:

$$E = \frac{\Delta\sigma_a}{\Delta\varepsilon_a} \approx 4.3 \text{ MPa} \quad (1)$$

$$\nu = \frac{\Delta\varepsilon_r}{\Delta\varepsilon_a} \approx 0.39 \quad (2)$$

$$G = \frac{E}{2(1+\nu)} \approx 1.5 \text{ MPa} \quad (3)$$

Those parameters correspond to a saturated clay type rock [29] and thus to the floor during the underground tests (Fig. 1a).

### 3. Results

#### 3.1. Optimisation of selected parameters of the base of shield support

A simplified numerical model of the base of shield support BW-16/34-POz produced by Becker-Warkop was developed. The basic technical parameters of the shield support are as follows:

- number of legs: 2;
- diameter of legs: 300 mm;
- permissible inclination, dir. front-back: 35°;
- permissible inclination, dir. right-left: ± 15°;
- advance: 0.8 m;
- set pressure: 25 MPa (1.77 MN).

The numerical model of the floor (Fig. 5) was made to be 10.0 m wide, 10.0 m long and 5.0 m high cuboid, created with 50 thousand balls (marked yellow). The support base was modelled in the form of two plates with various widths from 433 mm up to 779 mm and a constant length of 2300 mm. A rigid connection between the legs has been assumed and realised using the clump function (marked red). The point of force application resulting from the construction of the default shield support was formed as two additional balls (marked green) and provided a simulation of pressure increase from the two legs on the base. The pressure increase has been realised as a gradual increase of force from 0 MN up to 1.77 MN, corresponding to the set pressure of 25 MPa. Examples of the results obtained for the pressure increase of the shield support in operation on typical and weak floors are present in Fig. 6.

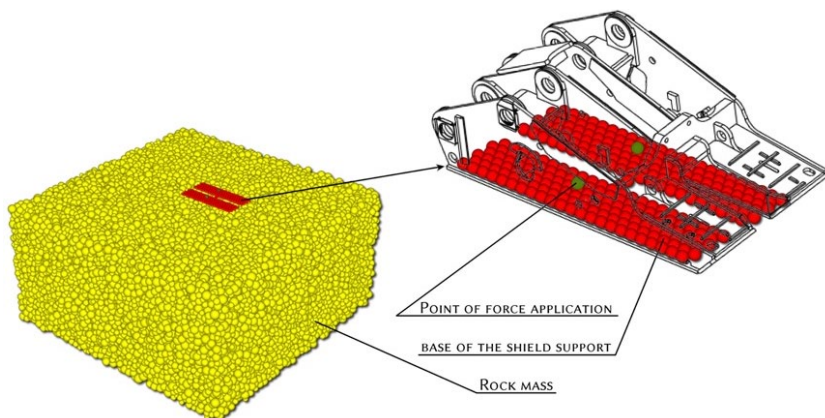


Fig. 5. Numerical model of the floor and the base of shield support used in calculations

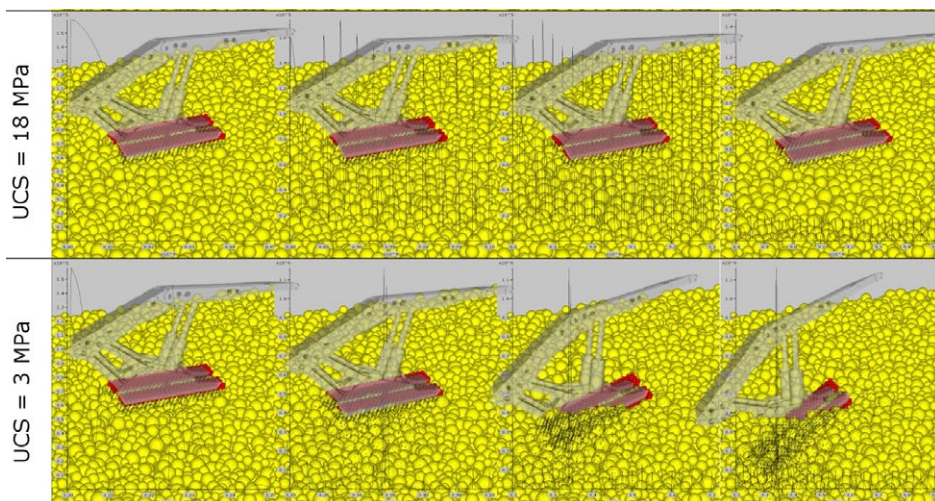


Fig. 6. Example of the simulation of the operation of a shield support with default a base width of 519 mm for different strength properties of the floor

The calculations conducted confirmed the importance of floor properties on the stability of functioning shield support. For a floor with high strength parameters, the support base remained stable in the whole range of exerted force. However, for a weak floor (UCS = 3 MPa), stability loss of the shield support was observed. In real conditions, the roof plane (not simulated in the model) limits the inclination of the shield support, as shown in Fig. 6. Nevertheless, the initial part of the simulation reproduced the correct sinking tendency of shield support on the weak floor.

In each of the analysed numerical models, the increase of leg pressure up to the set value (25 MPa) and the resulting changes of displacement in the four control points were monitored during the calculations. The control points were located on the extreme points of the base plates: front-left, front-right, back-left, back-right (Fig. 7).

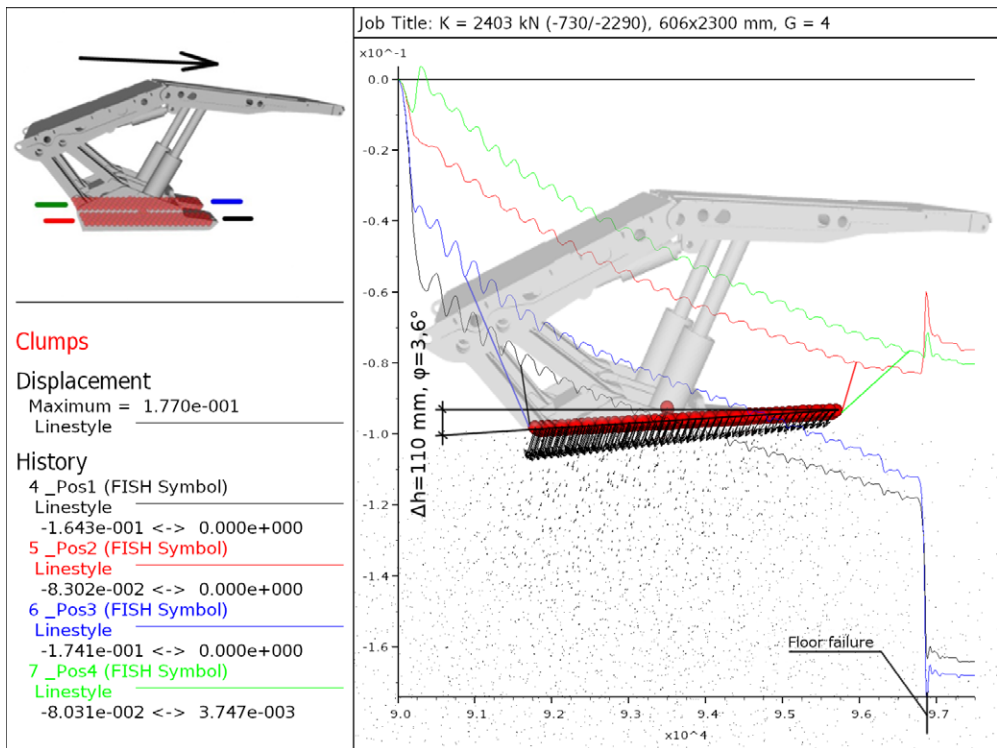


Fig. 7. Change in the displacement of control points on a base working on weak floor

The simulation of support advance was divided into three stages:

- gradual increase of the leg pressure up to the set pressure;
- the lifting of the shield support;
- the arrangement of the base parallel to the floor and advance of 0.8 m;
- repetition of previous steps.

An example of the results of the simulation of support advance is shown in Fig. 8, where the  $h_{\max}$  describes the maximal displacement of the base and  $\Delta h$  – the difference between the

displacement of front and back part of the base plates ( $\Delta h = 0$  means an arrangement parallel to the floor).

The calculations show that during operation on a weak floor, stability loss of the shield support must be taken into account, resulting from inclination both in the back-front and right-left

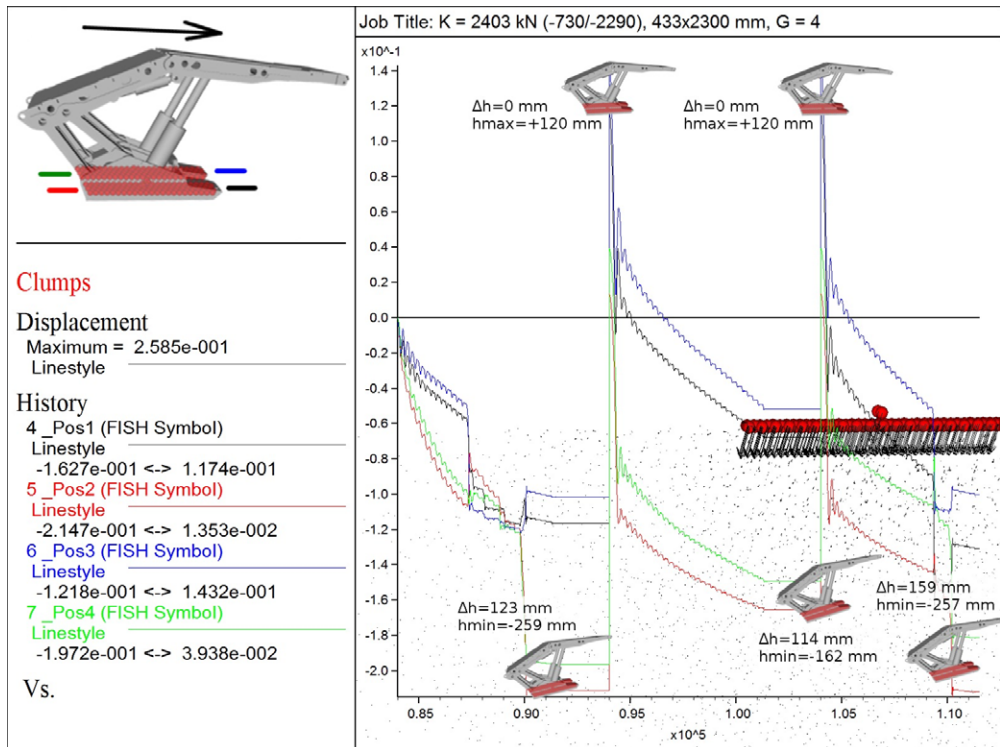


Fig. 8. Change in the displacement of control points on the base during a simulation of shield support advance (the shield support is not to scale)

direction. To improve the work of shield support, additional manual correction of the geometry of the shield support needs to be performed. Based on the similarity to the experience gathered from the underground observation of the shield support functioning on a weak floor, it has been assumed that the numerical model was positively verified.

### 3.2. Impact of the width of a shield support base on its interaction with a weak floor

Analysis of the impact of the base width on a shield support base's interaction with a weak floor (UCS = 3.0 MPa) was performed for five variants (Fig. 5):

- width of 2×433 mm;
- width of 2×519 mm (default width of the base);

- width of  $2 \times 606$  mm;
- width of  $2 \times 692$  mm;
- width of  $2 \times 779$  mm.

Results of the numerical calculations conducted to determine the optimum width of BW-16/34-POz shield support base for the assumed weak floor are presented in Figs 10 and 14.

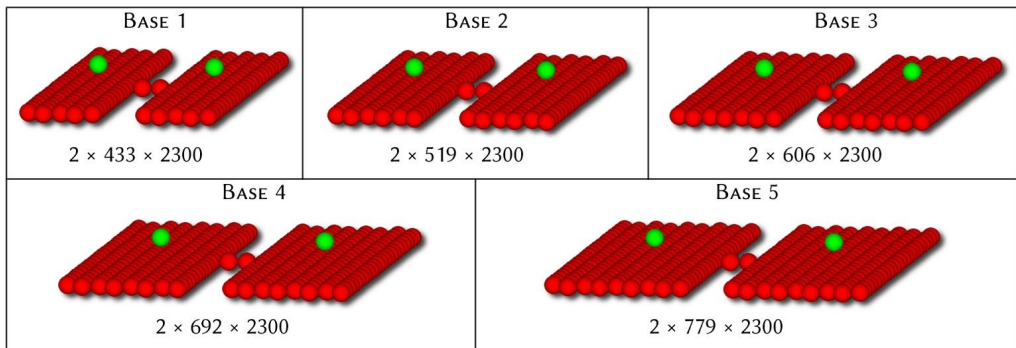


Fig. 9. Variants of the width of the support base assumed for calculations

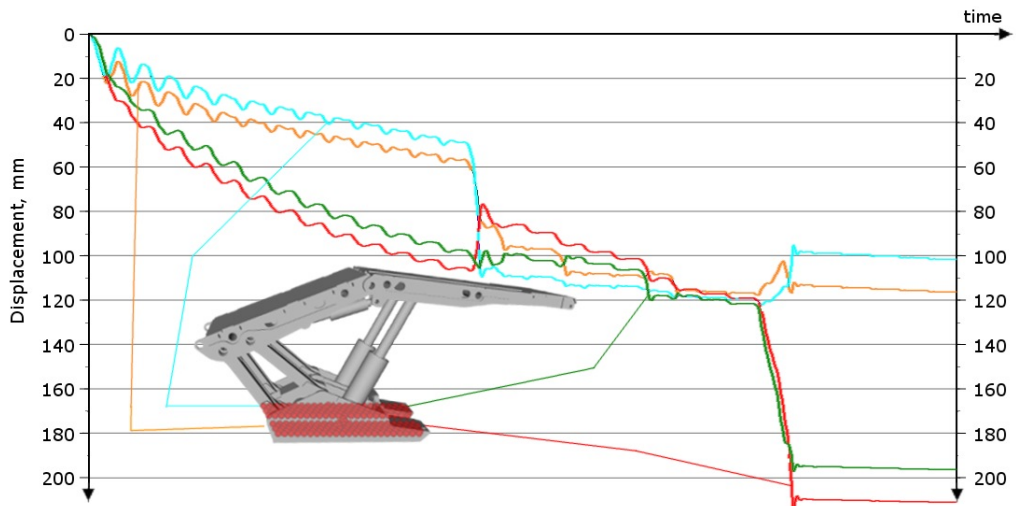


Fig. 10. Results of displacement calculations for support base of  $2 \times 433 \times 2300$  mm

The obtained results show that increasing the width of shield support has an advantageous influence on its stability in weak floor conditions. In a model of support with a 443 mm wide base, two sudden changes in the orientation of the base during the working of support were observed. In the initial phase of the work, the base showed a tendency to sink in the front section of the support, registered as a sudden displacement increase in the back section of the support base,

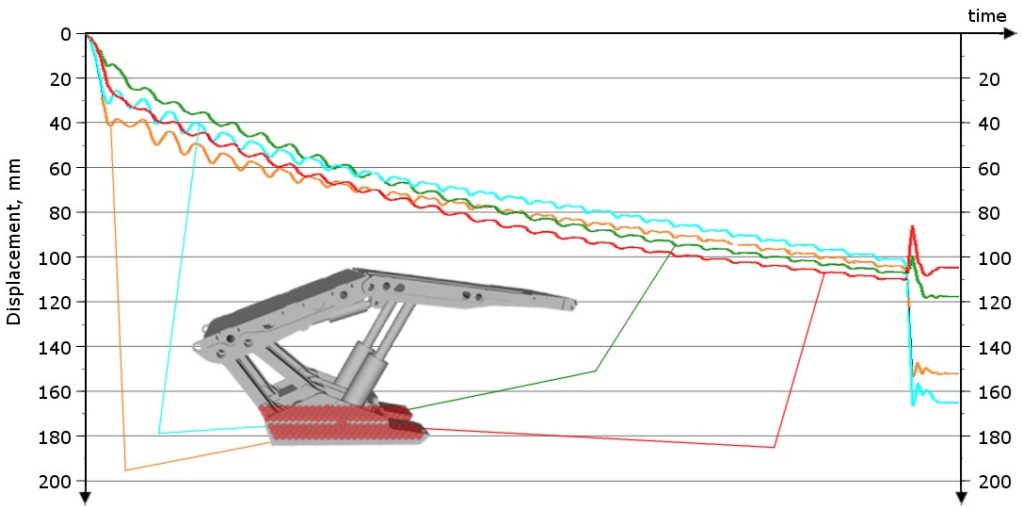


Fig. 11. Results of displacement calculations for support base of  $2 \times 519 \times 2300$  mm

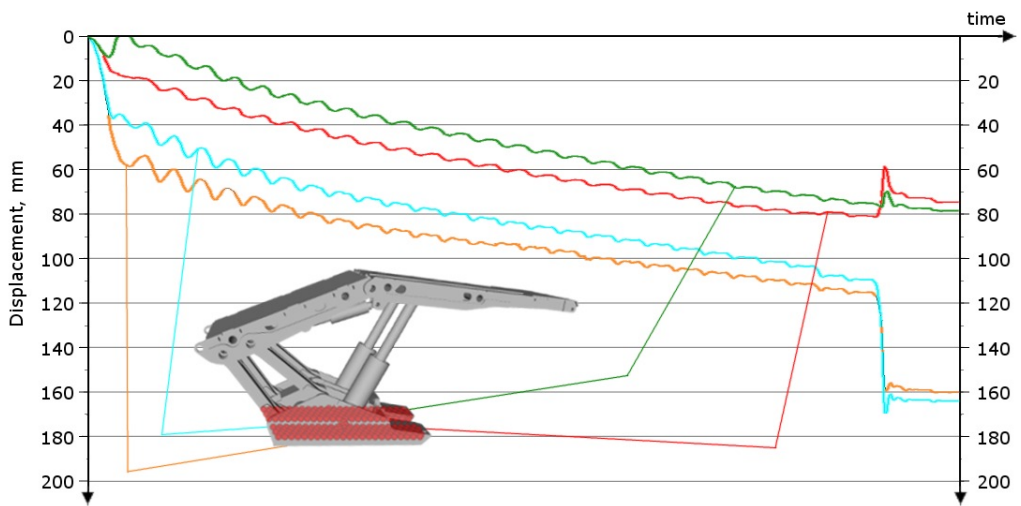


Fig. 12. Results of displacement calculations for support base of  $2 \times 606 \times 2300$  mm

followed by shortly stabilising and finally another rapid increase in displacement in the frontal part of the support base. The sudden increases in displacements were associated with two cases of local dynamic destruction of the floor in the area of increased pressure of the support base. Further numerical models showed that increasing the width of the support base results in reducing the number of local damage to the rock mass to just one occurrence (base width of 519 mm and 606 mm), and even prevents damage of the rock mass structure (no damage for a base with a width of 692 mm). Table 2 summarises the shield support geometry changes.

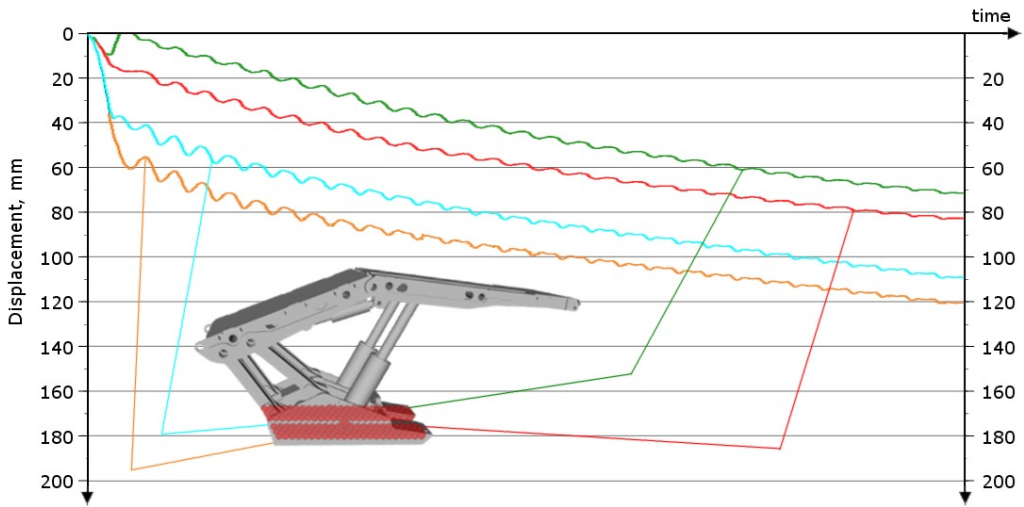


Fig. 13. Results of displacement calculations for support base of  $2 \times 692 \times 2300$  mm

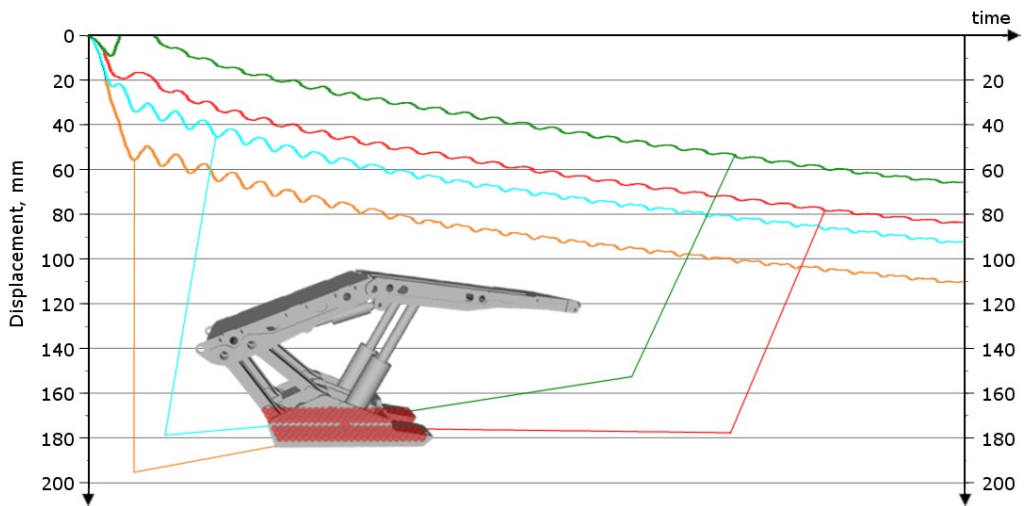


Fig. 14. Results of displacement calculations for support base of  $2 \times 779 \times 2300$  mm

TABLE 2

Results of the calculations of support with various width of the base

Parameter	Base dimensions, mm				
	2×433×2300	2×519×2300	2×606×2300	2×692×2300	2×779×2300
1	2	3	4	5	6
Front-Left displacement, mm	197.2	117.6	80.3	71.3	65.7
Front-Right displacement, mm	214.0	109.5	83.0	82.6	83.5

TABLE 2. Continued

	1	2	3	4	5	6
Back-Left displacement, mm	121.8	166.0	174.1	174.1	109.2	92.4
Back-Right displacement, mm	117.8	152.9	164.3	164.3	120.7	110.4
Mean displacement, mm	162.7	136.5	125.4	125.4	96.0	88.0
Inclination, dir. front-back °	-2.9	2.0	2.8	2.8	0.7	0.3
Inclination, dir. right-left (front), °	1.8	1.4	1.3	1.3	1.3	1.4
Inclination, dir. right-left (back), °	1.9	1.3	1.3	1.2	1.3	1.4

The data presented shows a tendency of the support in decreasing the incline both in the longitudinal plane (back-front direction) and transverse plane (left-right direction) due to the increase of the width of the base. The plot of maximal values of the displacement of the support is shown in in Fig. 15 and Fig. 16.

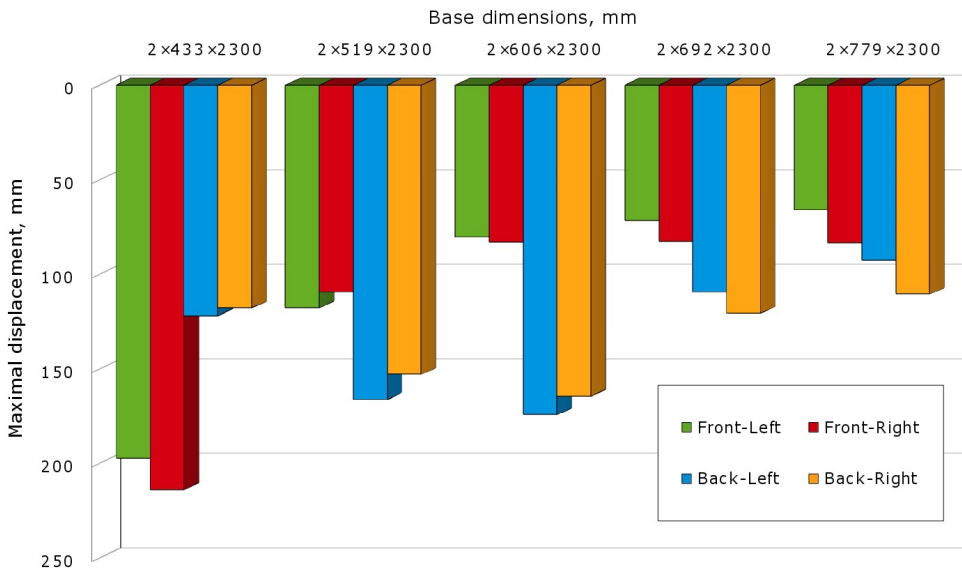


Fig. 15. Comparison of maximal displacements in control points for the analysed base of shield support

The result showed that the most important changes in the working conditions of the shield support occur for the base width below 692 mm. However, due to the construction limitation of the shield support, the resulting curve (Fig. 16) should be seen as a tendency only, and the next possible width of 606 mm should be treated as the optimal width of a base used on weak floors.

### 3.3. Impact of the location of hydraulic legs on the interaction of the base support with a weak floor

In further numerical studies, the impact of the location of force exerted on the base by hydraulic legs was analysed (Fig. 17). The analysis was conducted regarding the force applied in

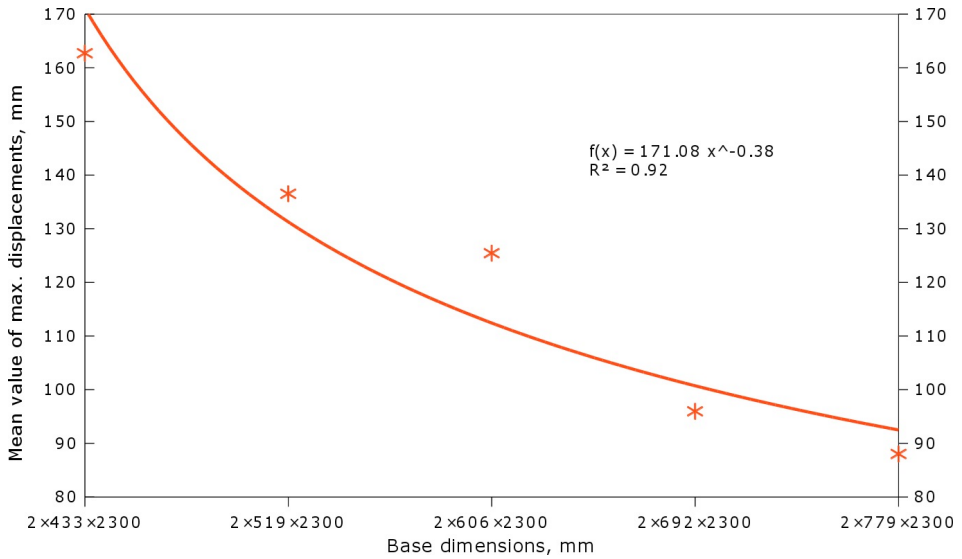


Fig. 16. Comparison of the maximal displacement for the analysed base of shield support

point P0 – determined on the underground measurements of a section of support working in the Janina coal mine, realised in the framework of the RFCS “GEOSOFIT [32]” project [33]. Results of the calculations are presented in Figs 18÷25.

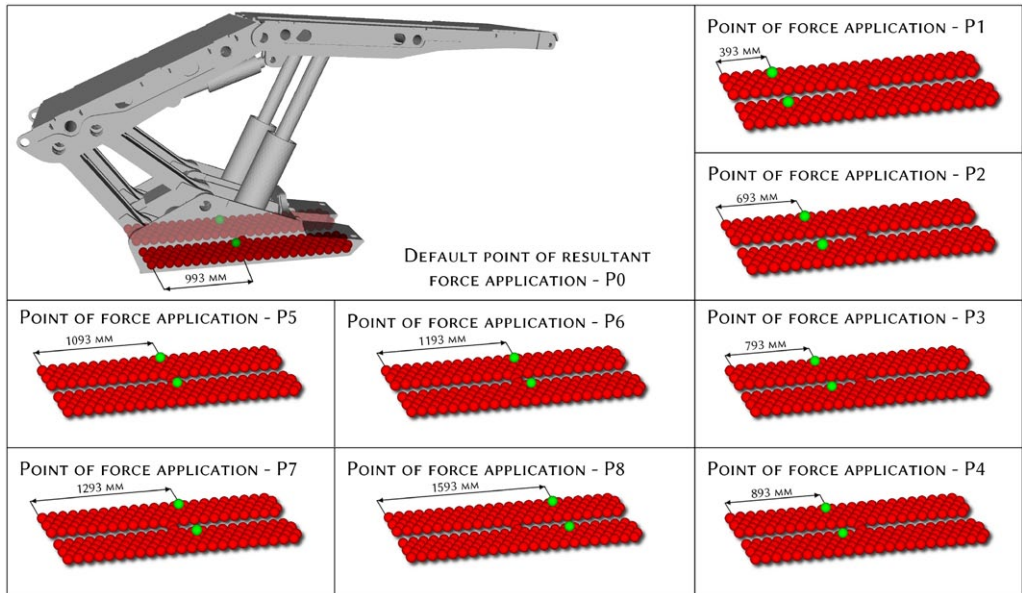


Fig. 17. Variants of point of resultant force application to the support base assumed for calculations

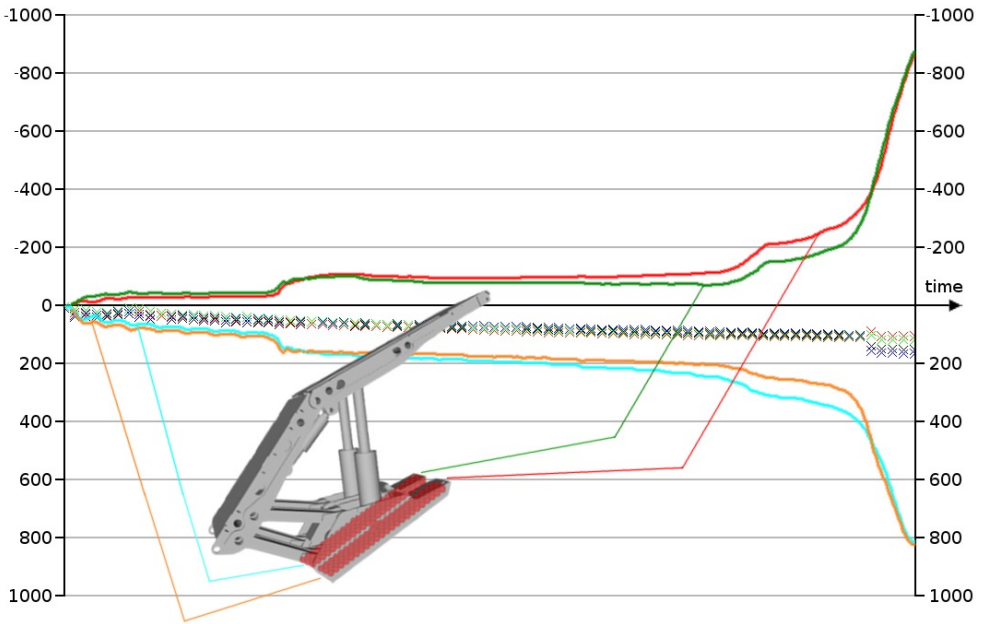


Fig. 18. Results of the calculations of displacement for the resultant force applied in point P1 (continuous line) and in point P0 (crosses)

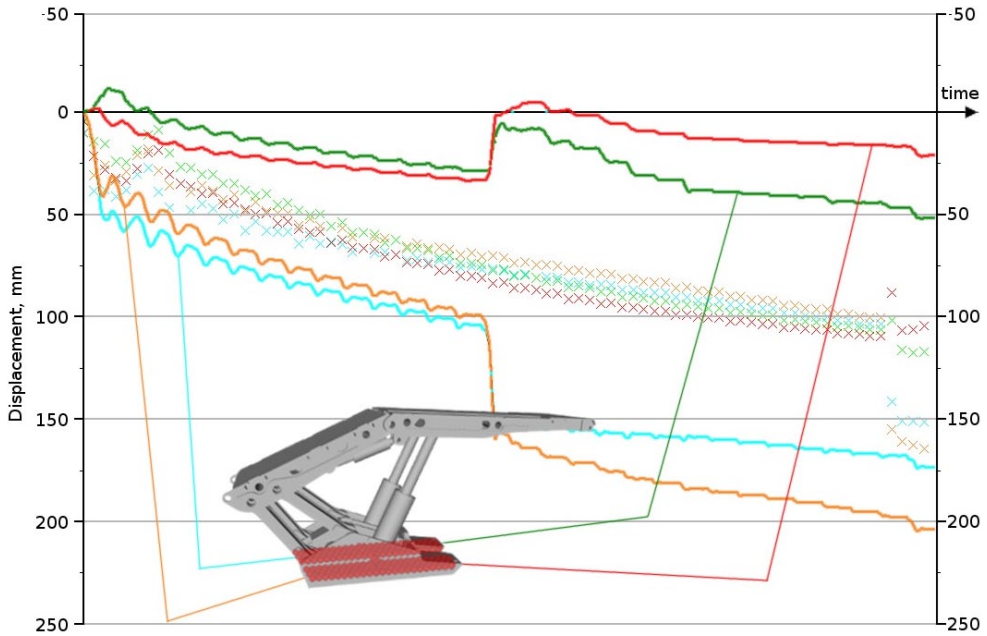


Fig. 19. Results of the calculations of displacements for the resultant force applied in point P2 (continuous line) and in point P0 (crosses)

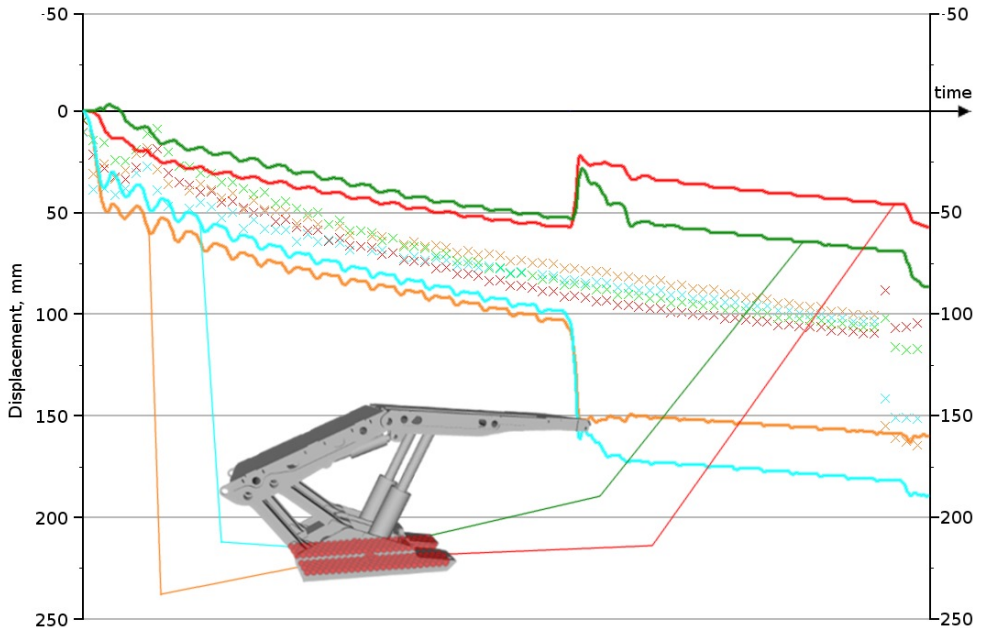


Fig. 20. Results of the calculations of displacements for the resultant force applied in point P3 (continuous line) and in point P0 (crosses)

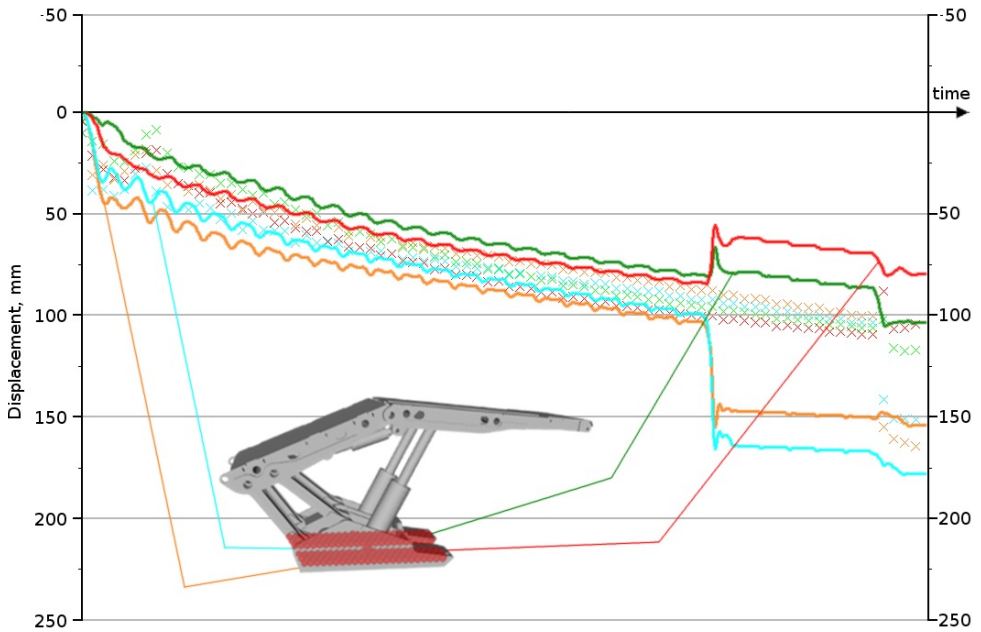


Fig. 21. Results of the calculations of displacements for the resultant force applied in point P4 (continuous line) and in point P0 (crosses)

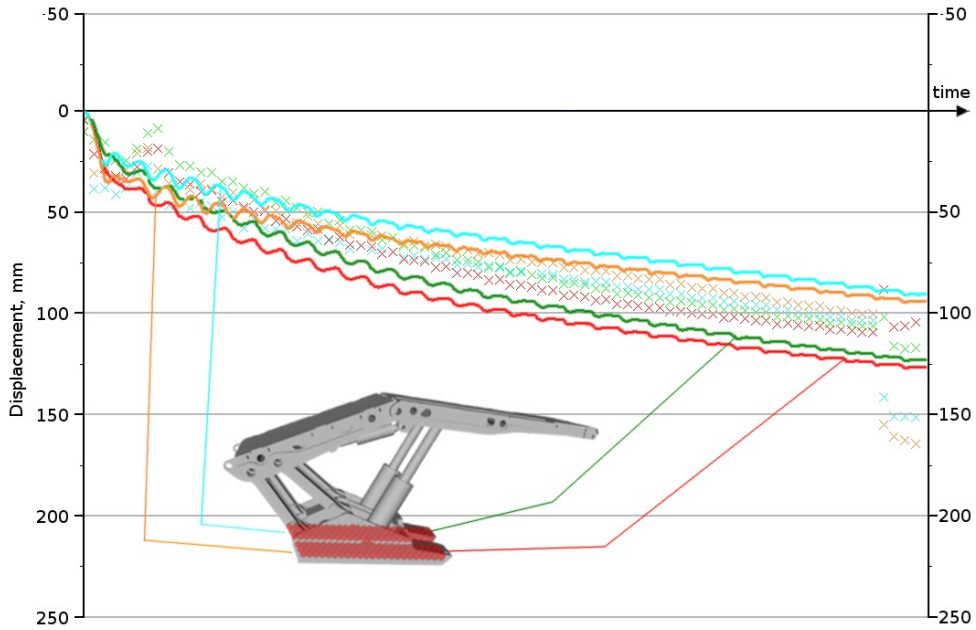


Fig. 22. Results of the calculations of displacements for the resultant force applied in point P5 (continuous line) and in point P0 (crosses)

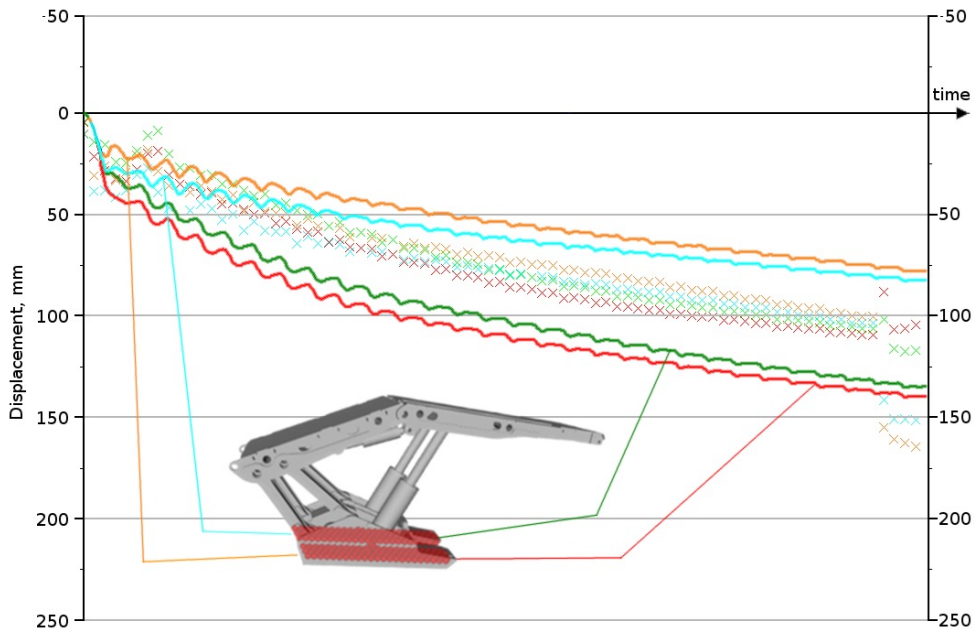


Fig. 23. Results of the calculations of displacements for the resultant force applied in point P6 (continuous line) and in point P0 (crosses)

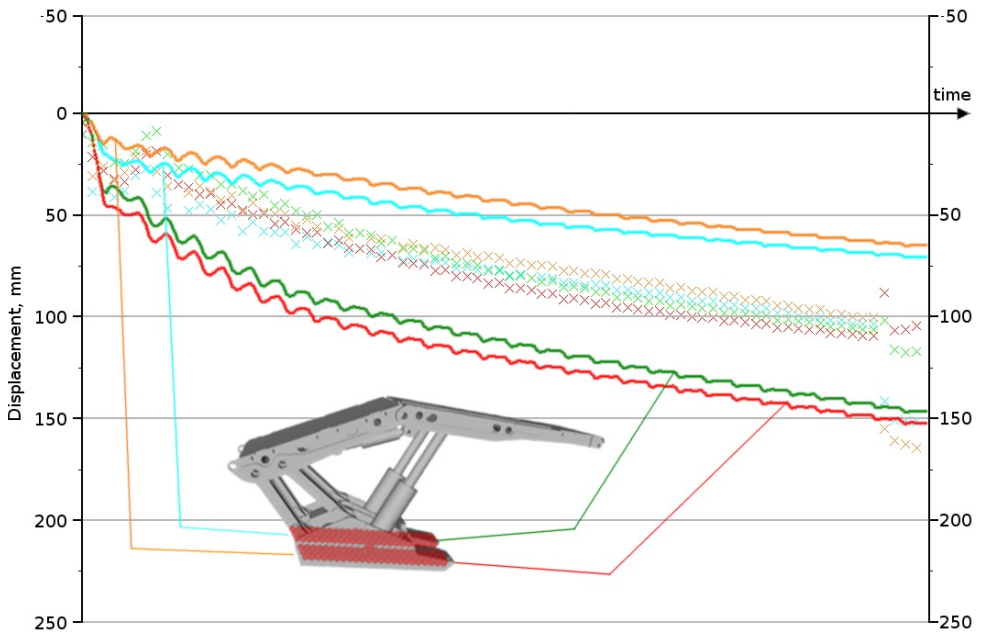


Fig. 24. Results of the calculations of displacements for the resultant force applied in point P7 (continuous line) and in point P0 (crosses)

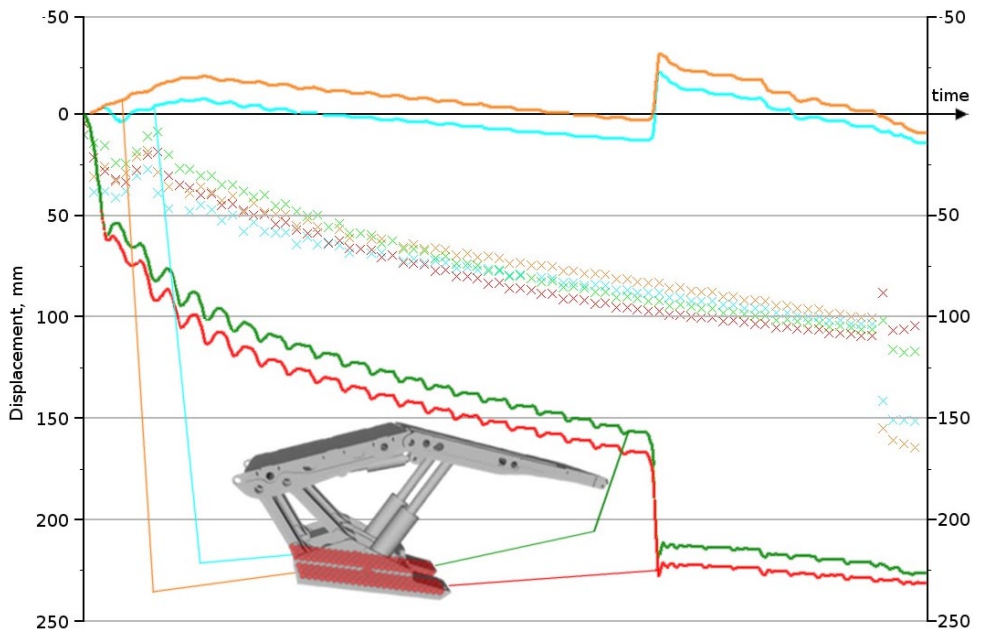


Fig. 25. Results of the calculations of displacements for the resultant force applied in point P8 (continuous line) and in point P0 (crosses)

The results show that moving the point of the resultant force application towards the back of the support base has a negative influence on the functioning of the support. In such cases, an increase in both displacements of the support and its tendency to incline were observed. A summary of the results is presented in Table 3 and Figs 26÷27.

TABLE 3

Results of calculations for various points of resultant force application

Parameter	Point of resultant force application, mm								
	P1 393	P2 693	P3 793	P4 893	P0 993	P5 1093	P6 1193	P7 1293	P8 1593
Front-Left displacement, mm	-877.4	52.2	86.9	105.6	117.9	123.7	135.6	147.2	226.9
Front-Right displacement, mm	-866.3	33.7	57.4	84.9	109.5	127.3	140.3	152.9	231.6
Back-Left displacement, mm	815.1	205.2	189.9	178.8	166.0	91.2	78.2	65.4	9.1
Back-Right displacement, mm	826.1	174.3	163.7	155.4	152.9	94.9	83.0	71.0	13.9
Mean displacement, mm	846.2	116.4	124.5	131.2	136.6	109.3	109.3	109.1	120.4
Inclination, dir. front-back, °	36.3	4.5	3.4	2.4	1.2	-0.9	-1.6	-2.2	-6.4
Inclination, dir. right-left (front), °	8.8	3.2	2.7	2.2	1.2	0.3	0.5	0.4	0.9
Inclination, dir. right-left (back), °	8.8	3.2	3.1	2.5	1.2	0.3	0.5	0.5	0.9

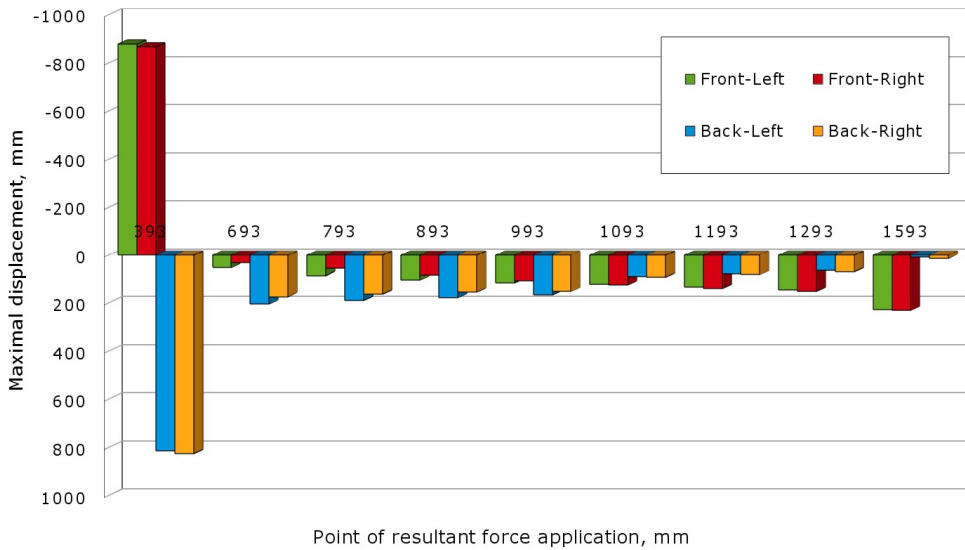


Fig. 26. Comparison of the base displacement for various points of force application

The data obtained show that the most favourable working conditions occurred when the point of force application was moved at point P5 (shifted by 100 mm toward the front of the base in relation to the default point P0). A further shift of the point of force application caused a slight decrease in the value of displacement and also resulted in the increased tendency of the shield support to inclination, especially in the longitudinal (back-front) direction.

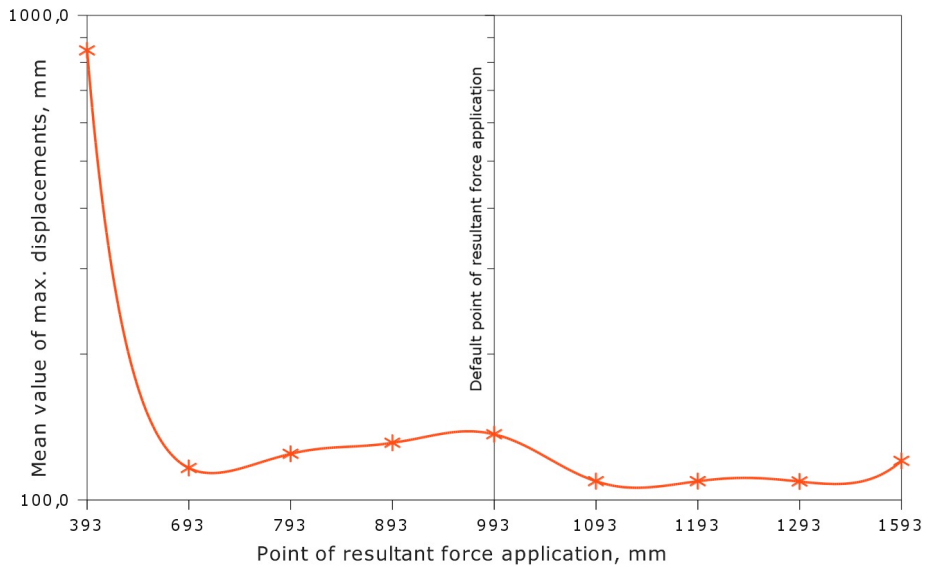


Fig. 27. Maximal displacement of the base for various points of force application

## 4. Summary

This paper presents an attempt to optimise selected parameters of the base of shield support functioning in conditions of a weak floor. The study was performed based on underground observations and numerical calculations using PFC3D. The results obtained enabled the analysis of the impact of the width of the base and the location of the spherical head connection to the base of the hydraulic legs on the interactions between the support and the floor. This led to the following conclusions:

- Construction of the powered shield support ought to ensure that the resultant pressure force of the base on the floor is as close to the centre of the base as possible.
- The location of the leg in the base and in the canopy influences the conditions of the interaction between the section and the rock mass. That is why, for given support, it is possible to determine optimum locations of spherical head connections.
- The width of the base of powered shield support ought to be properly designed for the geological and mining conditions to ensure the good interaction between the powered shield support and the rock mass.

## Acknowledgments

The numerical calculations presented were performed in the framework of the “GEOSOFT” project, co-financed by the Research Fund for Coal and Steel (Geomechanics and Control of Soft Mine Floors and Sides, RFCR-CT-2010-00001, 2010-2013).

## References

- [1] S. Prusek, S. Płonka, A. Walentek, Applying the ground reaction curve concept to the assessment of shield support performance in longwall faces. *Arabian Journal of Geosciences* **9** (3), p. 1-16 (2016). DOI: <https://doi.org/10.1007/s12517-015-2171-2>
- [2] S. Rajwa, The influence of the geometrical construction of the powered roof support on the loss of a longwall working stability based on the practical experience. *Arch. Min. Sci.* **65** (3), 511-529 (2020). DOI: <https://doi.org/10.24425/ams.2020.134132>
- [3] W. Masny, Powered support in dynamic load conditions – numerical analysis. *Arch. Min. Sci.* **65** (3), 453-468 (2020). DOI: <https://doi.org/10.24425/ams.2020.134129>
- [4] S. Rajwa, The impact of floor load-bearing capacity on the roof condition in the longwall face. *Przegląd Górniczy* **10**, 44-50 (2016).
- [5] S. Rajwa, T. Janoszek, S. Prusek, Influence of canopy ratio of powered roof support on longwall working stability – A case study, *International Journal of Mining Science and Technology* **29** (4), 591-598 (2019). DOI: <https://doi.org/10.1016/j.ijmst.2019.06.002>
- [6] S. Rajwa, T. Janoszek, S. Prusek, Model tests of the effect of active roof support on the working stability of a longwall. *Computers and Geotechnics* **118**, 103303 (2020). DOI: <https://doi.org/10.1016/j.compgeo.2019.103302>
- [7] J. Świątek, T. Janoszek, T. Cichy, K. Stoński, Computational Fluid Dynamics Simulations for Investigation of the Damage Causes in Safety Elements of Powered Roof Supports – A Case Study. *Energies* **14** (4), 1027 (2021). DOI: <https://doi.org/10.3390/en14041027>
- [8] P.M.V. Nguyen, T. Olczak, S. Rajwa, An investigation of longwall failure using 3D numerical modelling – A case study at a copper mine. *Studia Geotechnica et Mechanica*. **43** (4), 389-410 (2021). DOI: <https://doi.org/10.2478/sgem-2021-0019>
- [9] K. Terzaghi, R.B. Peck, G. Mesli, *Soil Mechanics In Engineering Practice*, 3rd Edition, John Wiley & Sons, Inc (1996).
- [10] D. Kumar, S.K. Das, An experimental study of the parameters influencing ultimate bearing strength of weak floor strata using physical modelling. *Geotechnical and Geological Engineering* **23** (1), 1-15 (2005). DOI: <https://doi.org/10.1007/s10706-003-3158-4>
- [11] M.M. Gadde, S.S. Peng, Weak Floor Stability During Perimeter Mining in the Illinois Basin Coal Mines. 28th International Conference on Ground Control in Mining, Morgantown, USA, 1-10 (2009).
- [12] S. Rajwa, W. Masny, S. Prusek, Powered Support in Conditions of Rock Mass Tremor Occurrence in the Polish Coal Mining. Aachen International Mining Symposium. 5th International Symposium – High Performance Mining (2009).
- [13] R. Frith, A holistic examination of the geotechnical design of longwall shields and associated mining risks. In: *Proceedings of the 13th Coal Operators' Conference*, 38-49 (2013).
- [14] S.S. Peng, *Longwall Mining*. 2nd Edition, Morgantown (2006).
- [15] M. Witek, Influence of rock strength parameters of floor on working conditions of powered roof support in the longwall face. PhD Thesis, Główny Instytut Górnictwa, Poland (2014).
- [16] S. Prusek, S. Rajwa, A. Wrana, A. Krzemień, Assessment of roof fall risk in longwall coal mines. *International Journal of Mining, Reclamation and Environment* **31** (8), 558-574 (2016). DOI: <https://doi.org/10.1080/17480930.2016.1200897>
- [17] C. Faria Santos, Z.T. Bieniawski, Floor Design In Underground Coal Mines. *Rock Mechanics and Rock Engineering* **22**, 249-271 (1989). DOI: <https://doi.org/10.1007/BF01262282>
- [18] R. Seedsman, The strength of the pillar-floor system. 12th Coal Operators' Conference, University of Wollongong & the Australasian Institute of Mining and Metallurgy 97-107 (2012).
- [19] M. Borecki, A. Kidybiński, Load capacity of the floor in coal seams. *Przegląd Górniczy* **3** (1964) (in Polish).
- [20] A. Barry, O.B. Nair, In Situ Testes of Bearing Capacity of Roof and Floor in Selected Bituminous Coal Mines. RI 7406 (1970).
- [21] D.W.H Su, R.O. Sceandrol, G. Hasenfus, Development and Evaluation of a Floor-Bearing Capacity Test Apparatus, 12nd Int. Conf. on Ground Control in Mining, 357-365 (1993).

- [22] A. Afrouz, Field and Bearing Capacity of Coal Mine Floor. *Int. J. Rock Mech. Min. Sci & Geomech.* **12**, 241-253 (1975).
- [23] G. Chen, Y.P. Chuch, Estimation of in situ viscoelastic parameters of weak floor strata by plate-loading testes. *Geotechnical and Geological Engineering* **14**, 151-167 (1996).
- [24] L. Prandl, Über die Härte plastischer Körper. *Nachrichten von der Königlichen Gesellschaft der Wissenschaften zu Göttingen. Mathematisch-physikalische Klasse* **1**, 74-85 (1920).
- [25] M. Hjiiaj, A.V. Lyamin, S.W. Sloan, Bearing capacity of a cohesive-frictional soil under non-eccentric inclined loading. *Computers and Geotechnics* **31** (6), 491-516 (2004). DOI: <https://doi.org/10.1016/j.compgeo.2004.06.001>
- [26] M. Hjiiaj, A.V. Lyamin, S.W. Sloan, Numerical limit analysis solutions for the bearing capacity factor. *International Journal of Solids and Structures* **42** (5-6), 1681-1704 (2005). DOI: <https://doi.org/10.1016/j.ijsolstr.2004.08.002>
- [27] Z. Wiłun, *Outline of geotechnics*. Wydawnictwa Komunikacji i Łączności WKŁ, Warszawa, Poland (2005).
- [28] J.A. Nemcik, *Floor failure mechanisms at underground longwall face*. University of Wollongong (2003).
- [29] P. Małkowski, A. Ulaszek, Ł. Ostrowski, Optimization of roof coal thickness in the roof of longwall face as a result of water inflow into roof rocks. *Przegląd Górniczy* **3**, 48-57 (2014).
- [30] J. Markowicz, S. Rajwa, S. Szewda, Modelling of Powered Roof Support Cooperation with the Floor of Low Bearing Capacity in the Aspect of Shaping the Section Design. *Archives of Mining Sciences* **62** (1), 177-188 (2017). DOI: <https://doi.org/10.1515/amsc-2017-0013>
- [31] PFC3D, User Manual. Itasca Consulting Group, Minneapolis, MN, USA.
- [32] GEOSOFTE, Geomechanics and control of soft mine floors and sides. Project co-financed by Research Fund for Coal & Steel. Project no. RFCR-CT-2010-00001, realization in 2010-2013 (not published).
- [33] S. Prusek, S. Rajwa, W. Kasperkiewicz, T. Budniok, Assessment of performance of powered shield support used on weak floor. *World Mining Congress* (2013).